Single Doppler Velocity Signature Interpretation of Nondivergent Environmental Winds

VINCENT T. WOOD AND RODGER A. BROWN

National Severe Storms Laboratory, Norman, OK 73069

(Manuscript received 8 February 1985, in final form 24 July 1985)

ABSTRACT

A variety of single Doppler velocity patterns that simulate those observed in a nondivergent environment is presented. Measurements in optically clear air and/or widespread precipitation are simulated, using horizontally uniform wind fields that vary with height. Vertical profiles of wind speed and direction indicated by the simulated Doppler velocity fields agree well with Doppler radar measurements. Horizontally uniform winds veering with height produce a striking S-shaped pattern, indicative of warm air advection; winds backing with height produce a backward S, indicative of cold air advection. A maximum in the vertical profile of wind speed is indicated by a pair of concentric contours, one upwind and one downwind of the radar. The presence of a frontal discontinuity is indicated by rapid variation of wind direction within the frontal zone. The wind speed profile controls the overall pattern including the spacing between contours, whereas the vertical profile of wind direction controls contour curvature.

1. Introduction

During the mid-1970s government agencies with severe storm warning concerns—National Weather Service (NWS), U.S. Air Force's Air Weather Service (AWS), Federal Aviation Administration (FAA)—became increasingly interested in the capabilities of Doppler radar (e.g., Johannessen and Kessler, 1976). This interest led to the establishment of the Joint Doppler Operational Project (JDOP) during 1977–79 to test Doppler radar in an operational setting. The results prepared by JDOP Staff (1979) were so encouraging that the agencies decided to replace their aging weather radars with the jointly procured Next Generation Weather Radar (NEXRAD), which includes Doppler capability (e.g., Bonewitz, 1981; Ray and Colbert, 1982).

The efficient use of NEXRAD base products by operational nowcasters/forecasters requires physical understanding and recognition of certain meteorological signatures found in reflectivity and Doppler velocity fields. Of importance is the wide variety of weather features that can be identified readily by means of color displays (e.g., Gray et al., 1975; Kraus and Donaldson, 1976; Baynton et al., 1977; Locatelli and Hobbs, 1978; Baynton, 1979; Wilson et al., 1980; Wilson, 1982). Among these features are the vertical variation of wind in widespread precipitation, frontal boundaries, gust fronts, tornadoes, hurricane winds, wind shear hazardous to aircraft, and winds in the optically clear boundary layer.

Real-time information on the vertical variation of wind in optically clear air and/or widespread precipitation has been a subject of increasing interest. Lhermitte and Atlas (1961) described how a single Doppler radar could be used to measure profiles of wind velocity in widespread precipitation. Their VAD (Velocity–Azimuth Display) technique involves rotation of the antenna while it is directed at a constant elevation angle to record radial velocity of precipitation particles at a fixed range. Timely wind information obtained by the VAD technique is used to compute wind direction and speed, divergence, vertical velocity, and deformation (Browning and Wexler, 1968; Rabin and Zrnić, 1980, among others).

Studies by Kraus and Donaldson (1976), Baynton et al. (1977), Wilson et al. (1980), and Wilson (1982) discuss techniques for recognizing and interpreting single Doppler velocity patterns that provide a variety of real-time information about the atmosphere. Nevertheless, it may not be clear how temporal variations in the vertical profiles of wind speed and direction alter real-time Doppler color displays. For instance, how does an observer readily recognize and interpret the color displays when vertical profiles of wind speed and/or wind direction are evolving with time?

Our purpose here is to answer that question by providing simulated single Doppler velocity patterns for a variety of vertical wind profiles in a horizontally homogeneous environment; similar fields have been discussed by Wood and Brown (1983). Patterns are produced for wind profiles that become increasingly complex. These patterns readily aid recognition and interpretation of such wind fields. Further, patterns are portrayed with contour lines of equal Doppler velocity spacing; these lines represent the boundaries between

adjacent colors (velocity intervals) on a color display. Simulations also are compared with actual Doppler velocity measurements.

2. Simulation model

When a Doppler radar samples the atmosphere, it measures only the component of the wind in the direction that the radar's antenna is pointing. In the case of a uniform horizontal wind, the Doppler velocity value changes continuously with changing viewing direction. When the antenna is pointing directly upwind or downwind, the full wind is measured. However, only a fraction of that amount is measured in other directions; and Doppler velocity is zero when the antenna is pointing normal to the wind. What might appear to be a very frustrating situation is, in fact, relatively easy to interpret when Doppler velocity measurements in all directions are viewed as one composite picture. We present such composite pictures along with the hypothetical wind fields that produced them.

To develop the simulation model, let us consider a Cartesian coordinate system in which x and y are horizontal distances from a Doppler radar site (Fig. 1). As an antenna rotates about a vertical axis z at a constant elevation angle ϕ, detailed displays are obtained of the Doppler component of the target velocity V_d as a function of azimuth θ and slant range r_s (or height h). We now discuss procedures for computing vertical profiles of horizontally homogeneous wind direction and speed.

A Doppler radar detects only the component of wind velocity along the radar beam. From the simplified flat earth geometry in Fig. 1a it is seen that, since $h = r_s \times \sin\phi$ and $H = R_s \sin\phi$,

$$\frac{r_s}{R_s} = \frac{h}{H}, \tag{1}$$

where r_s is the slant range from the radar site, R_s the maximum slant range at the edge of the radar display, h the height above the radar's horizontal plane, and H the maximum height at the edge of the display. The wind components in the idealized environmental flow fields are used to compute Doppler components relative to the radar. With velocity component u directed eastward and component v directed northward, the Doppler component of wind toward or away from the radar, denoted by V_d, is computed from the simple expression

$$V_d = u\cos\phi\sin\theta + v\cos\phi\cos\theta + w\sin\phi. \tag{2}$$

For horizontally uniform (nondivergent) wind fields, where w is zero, Eq. (2) becomes

$$V_d = u\cos\phi\sin\theta + v\cos\phi\cos\theta. \tag{3}$$

Note that Eq. (3) is also valid for nonuniform wind fields ($w \neq 0$) as long as the elevation angle ϕ is small enough that the vertical velocity component will be negligibly small compared with the horizontal wind components. The general form of the wind components used to profile tropospheric winds is given by

$$u = \text{spd}(h)\cos[270° - \text{dir}(h)]$$
$$v = \text{spd}(h)\sin[270° - \text{dir}(h)], \tag{4}$$

where spd(h) is the wind speed, dir(h) is the wind direction, and both are functions of height, h. It is easily verified that the homogeneous horizontal wind field is entirely nondivergent; i.e.,

$$\frac{\partial u}{\partial x} + \frac{\partial v}{\partial y} = 0. \tag{5}$$

General expressions of the nth-degree polynomial used to describe various wind regimes in the wind speed and direction profiles are

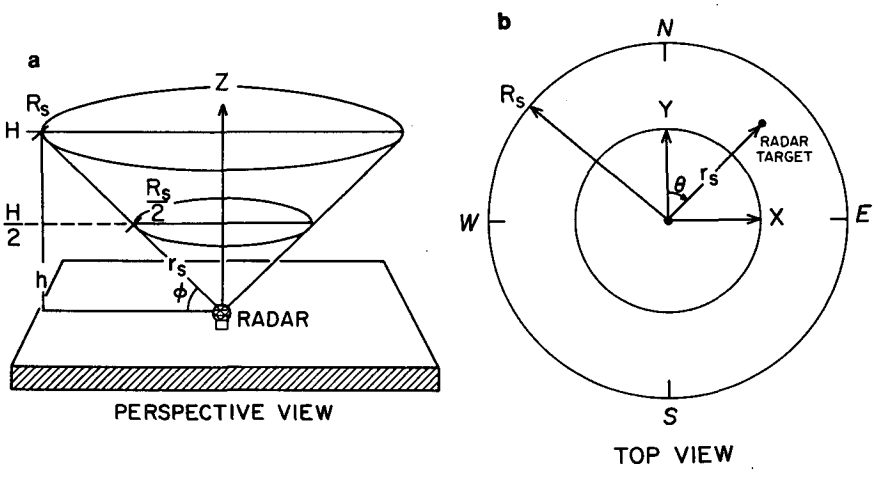

FIG. 1. Doppler radar viewing configuration. (a) Radar scanning around vertical axis, z, at a constant elevation angle, ϕ; (b) view of (a) from the top, representing a PPI (plan position indicator) scope.

$$\left.\begin{aligned} \text{spd}(h) &= S\left[\sum_{i=0}^{n} a_i\left(\frac{h}{H}\right)^i\right] \\ \text{dir}(h) &= \theta\left[\sum_{i=0}^{n} b_i\left(\frac{h}{H}\right)^i\right] \end{aligned}\right\}, \quad 0 \leqslant h \leqslant H, \qquad (6)$$

where a_i and b_i ($i = 0, 1, 2, \cdots, n$) are constants, and S and θ are the prescribed wind speed and direction, respectively. The expressions in Eq. (6) can be either linear or nonlinear, depending upon the arbitrarily prescribed profiles of the wind speed and direction. Consider, for example, a profile with constant wind speed and a wind direction that veers linearly with height. The corresponding expressions of the zero- and first-degree polynomials for spd(h) and dir(h) are, respectively,

$$\left.\begin{aligned} \text{spd}(h) &= S \\ \text{dir}(h) &= 180°\left[1 + 0.5\left(\frac{h}{H}\right)\right] \end{aligned}\right\}, \quad 0 \leqslant h \leqslant H. \qquad (7)$$

As an example of how to interpret Fig. 1 and Eqs. (3), (4) and (7), consider the wind field and associated Doppler velocity pattern in Fig. 2. At the radar location in the center of the PPI scope, the wind is from the south (Fig. 2a). As the elevated radar beam passes upward through the atmosphere, the wind direction changes linearly through south-southwesterly to westerly at the edge of the display scope. The corresponding Doppler velocity measurements are shown in Fig. 2b. At the outer edge of the display, where the environmental winds are from the west, the Doppler velocity component is zero (heavy long dashes) when the radar points north or south, perpendicular to the wind direction. When the radar points east, maximum flow away from the radar (heavy solid line) is measured; when the radar points west, maximum flow toward the radar (heavy dotted line) is measured. At the middle-range circle, where the wind is from the southwest, the Doppler component is zero when the radar points northwest or southeast; extreme Doppler velocity components toward and away from the radar are measured when the radar points southwest and northeast, respectively. Using the same lines of reasoning at other ranges from the radar (representing heights above ground), we note that the zero Doppler velocity contours and, in fact, all Doppler component contours become S-shaped lines. Thus, we have in Fig. 2b a unique Doppler velocity pattern representing an environmental wind profile where wind speed is constant and wind direction varies linearly from southerly at the ground through southwesterly to westerly at the edge of the display.

3. Uniform flow at all heights

We consider three uniform flow fields (wind direction and speed remain constant with height) whose vertical profiles are described by

$$\begin{aligned} &\text{(a)}\ \text{spd}(h) = S \quad \text{dir}(h) = 225° \qquad \text{(b)}\ \text{spd}(h) = S \quad \text{dir}(h) = 270° \\ &\text{(c)}\ \text{spd}(h) = S \quad \text{dir}(h) = 315° \qquad 0 \leqslant h \leqslant H, \end{aligned} \qquad (8)$$

where S is the unspecified constant wind speed. These data are illustrated in Fig. 3. Vertical profiles of hy-

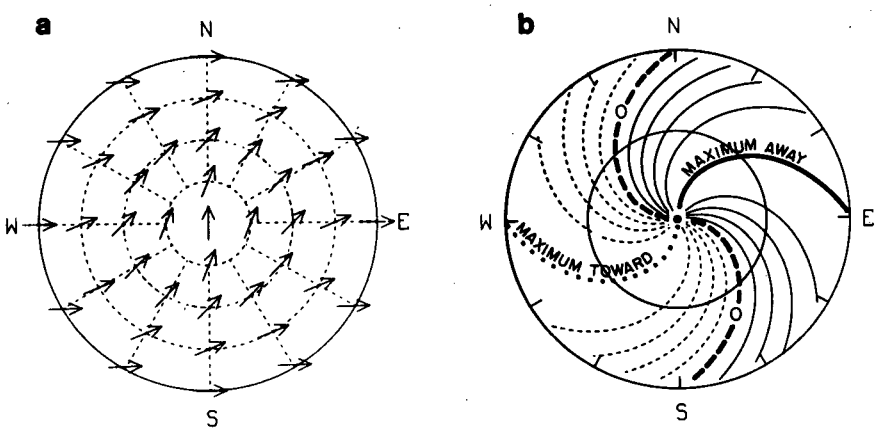

FIG. 2. Plan view of (a) wind field and (b) corresponding single Doppler velocity contours along an inverted conical surface (constant elevation angle) with the radar at the apex (center) as shown in Fig. 1a. The wind direction changes linearly from south at the radar location through southwest to west at the edge of the radar collection region; wind speed is constant throughout. Solid contours represent flow away from the radar, short dashes represent flow toward the radar, and heavy long dashes represent zero Doppler velocity. Heavier solid and dotted lines indicate locations of extreme Doppler velocity values within the display. The spacing between contour lines represents constant Doppler velocity intervals.

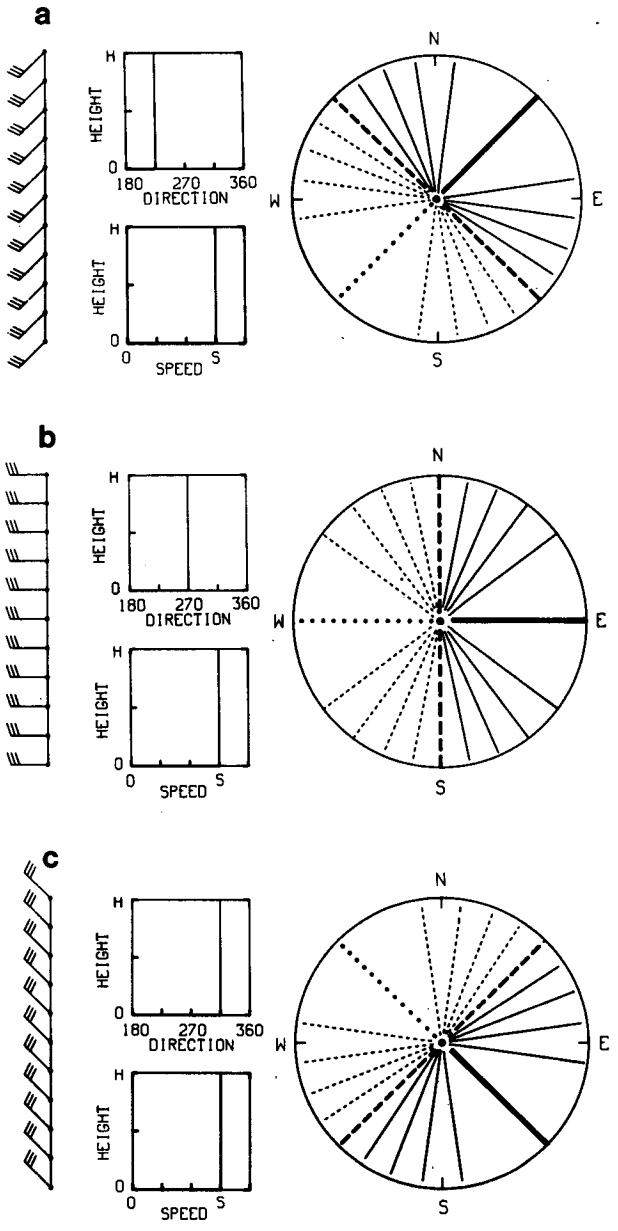

FIG. 3. Vertical profiles of uniform horizontal wind fields and corresponding Doppler velocity patterns (as seen on a PPI scope) for winds blowing from (a) 225°, (b) 270° and (c) 315°. Solid lines represent flow away from the radar; short dashes represent flow toward the radar; heavy long dashes represent zero Doppler velocity. Heavier solid and dotted lines indicate locations of maximum and minimum Doppler velocity values within the display. The thick long-dashed contour represents zero Doppler velocity where the radar beam is oriented perpendicular to the wind direction. Contour interval is 0.2 S.

pothetical wind direction and speed computed from Eqs. (4) and (8) are shown, respectively, in the upper and lower boxes in the middle part as well as portrayed by conventional wind symbols in the left part of these figures. Thus, for instance, Fig. 3a shows that the wind is from the southwest (225°) at a constant speed S at all altitude levels. The radar measures zero velocity component when it points toward 135° and 315° azimuth. At these azimuths, the radar beam is oriented perpendicular to the wind direction at all altitudes and therefore at all slant ranges. As the radar rotates clockwise away from 315° (135°) the Doppler velocity increases (decreases) until it reaches a maximum value of the wind speed S at 45° (minimum of $-S$ at 225°). At these azimuths, the radar beam is oriented parallel to the wind direction and therefore measures a Doppler velocity component equal in magnitude to the wind speed.

Figures 3b and 3c represent constant wind direction and speed situations in which the wind direction is 270° (Fig. 3b) and 315° (Fig. 3c). Interpretation of the Doppler displays in Figs. 3b and 3c is similar to that of Fig. 3a, except that in each figure the pattern rotates clockwise by 45° for each step.

4. Uniform directional shear with constant wind speed

A wind structure in which the wind direction changes uniformly with height and the wind speed remains invariant is represented by arbitrary vertical profiles for backing (cold air advection) and two strengths of veering (warm air advection) winds given by

$$\left.\begin{aligned}
&\text{(a)}\ \mathrm{spd}(h) = S \\
&\qquad \mathrm{dir}(h) = 180° - 0.25\left(\frac{h}{H}\right) \\
&\text{(b)}\ \mathrm{spd}(h) = S \\
&\qquad \mathrm{dir}(h) = 180° + 0.25\left(\frac{h}{H}\right) \\
&\text{(c)}\ \mathrm{spd}(h) = S \\
&\qquad \mathrm{dir}(h) = 180° + 0.5\left(\frac{h}{H}\right)
\end{aligned}\right\}, \quad 0 \leq h < H. \tag{9}$$

These profiles are correspondingly illustrated in Fig. 4. Figure 4a exhibits backing of the wind with height up to the maximum height H. Note that the zero velocity contour (thick long-dashed) bisects the radar display in the shape of a "backward S." Since the zero contour represents flow perpendicular to the radar viewing direction (from dashed toward solid contours), the pattern indicates a southerly wind at the surface, backing with height until it becomes southeasterly at the edge of the radar display.

In Fig. 4b, the radar display is comparable with that of Fig. 4a, except that the pattern is reversed so that the display is bisected by a letter "S." The zero velocity

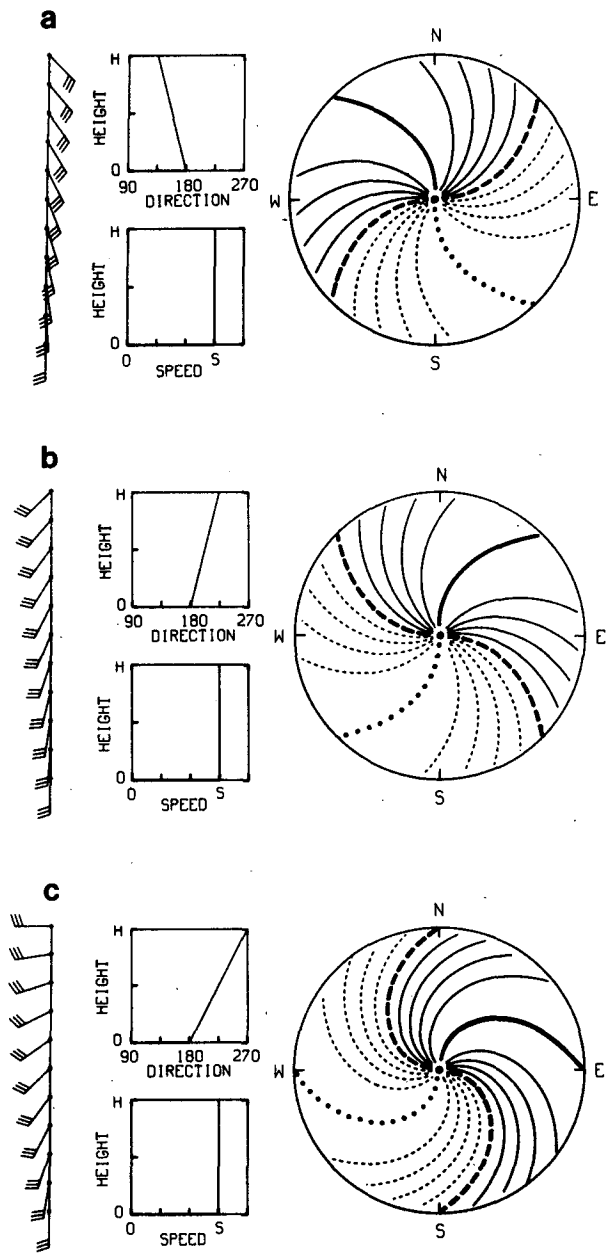

FIG. 4. Uniform directional shear with constant wind speed: (a) backing wind, (b) veering wind and (c) stronger veering of wind. Doppler velocity contours as in Fig. 3.

contour shows winds veering from south near the surface to southwest aloft.

The velocity components exhibit greater curvature in Fig. 4c than in Fig. 4b because of the more rapid changing wind direction with height. It is obvious that greater curvature of the Doppler velocity contours implies increased veering of the winds. We note, by following the zero velocity contour, that winds veer from southerly near the ground to westerly aloft.

5. Uniform wind speed shear with constant wind direction

Figure 5 illustrates wind regimes where wind speed changes linearly with height while wind direction does not change. Note that a circle located at the bottom of vertical wind sounding in Fig. 5a denotes calm winds at the surface. Three vertical profiles describing the degree to which the wind speed changes linearly with height are given, corresponding to

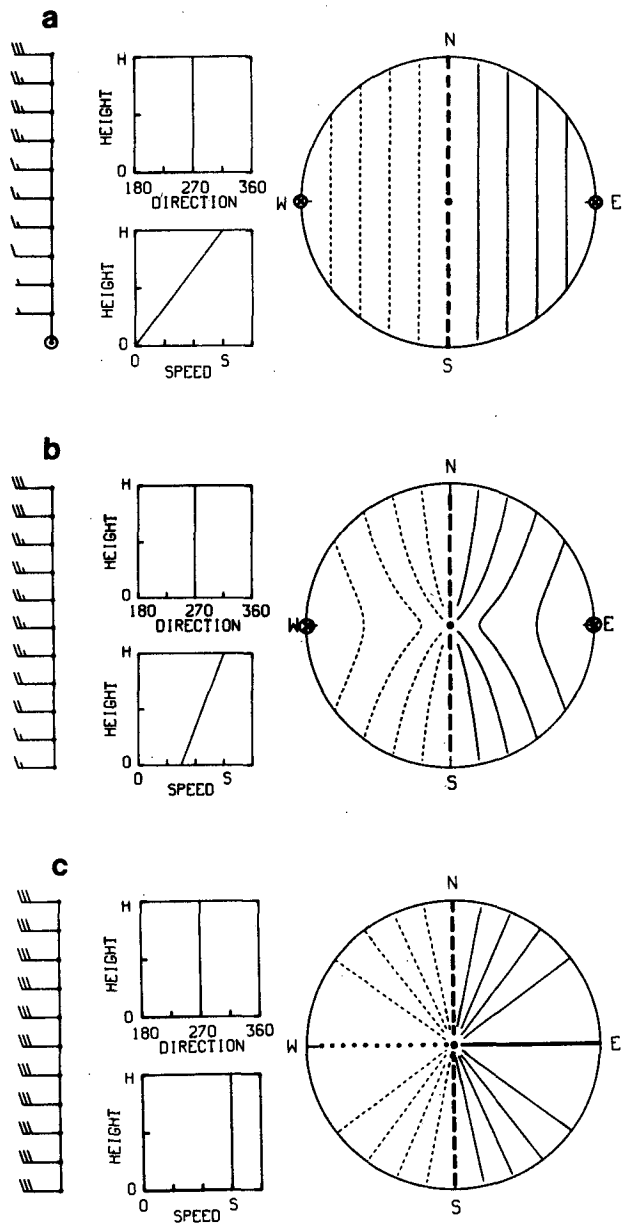

FIG. 5. Uniform wind speed shear with constant wind direction. Doppler velocity contours as in Fig. 3. Circled X's indicate locations of maximum and minimum Doppler velocity values within the display.

$$\left.\begin{aligned}
&\text{(a)}\ \text{spd}(h) = S\left(\frac{h}{H}\right)\\
&\qquad \text{dir}(h) = 270^\circ\\
&\text{(b)}\ \text{spd}(h) = S\left[0.5 + 0.5\left(\frac{h}{H}\right)\right]\\
&\qquad \text{dir}(h) = 270^\circ\\
&\text{(c)}\ \text{spd}(h) = S\\
&\qquad \text{dir}(h) = 270^\circ
\end{aligned}\right\},\ 0 \leq h \leq H. \quad (10)$$

Note in Fig. 5a that when the wind direction is uniform and wind speed increases from zero linearly with height, the contours are straight lines oriented parallel to the zero velocity contour. Extreme Doppler velocity values are indicated by circled ×'s on the edge of the radar display, one upwind and one downwind; these extrema occur at one height rather than at all heights as was the case in the preceding figures.

The westerly wind shear in Fig. 5b is less than that in Fig. 5a; wind speed at the ground is one half of the maximum value S (instead of being zero). The thin solid and short-dashed contours tend to converge at the center of the radar display and are no longer parallel to the zero velocity contour. The zero velocity contour remains unchanged with height (range) because wind direction is constant.

If the surface wind speed exceeds that in Fig. 5b, then an increasing number of contour lines meet at the center of the display. It is apparent that the stronger the surface winds are, the more rapidly the contours converge until they become straight lines (Fig. 5c) when both wind speed and direction are constant with height.

6. Nonuniform directional shear with constant wind speed

A nonlinear variation of wind direction with height (range) can be simulated using a parabolic profile. Three vertical profiles are described by

$$\left.\begin{aligned}
&\text{(a)}\ \text{spd}(h) = S\\
&\qquad \text{dir}(h) = 180^\circ\left[1 - \frac{h}{H}\left(1 - \frac{h}{H}\right)\right]\\
&\text{(b)}\ \text{spd}(h) = S\\
&\qquad \text{dir}(h) = 180^\circ\left[1 + \frac{h}{H}\left(1 - \frac{h}{H}\right)\right]\\
&\text{(c)}\ \text{spd}(h) = S\\
&\qquad \text{dir}(h) = 180^\circ\left[1 + 2\frac{h}{H}\left(1 - \frac{h}{H}\right)\right]
\end{aligned}\right\},\ 0 \leq h \leq H. \quad (11)$$

These profiles are represented in corresponding Figs. 6a–c. Again, the zero velocity contour traces a letter "S" (backward "S") when winds veer (back) with height. Figure 6a shows a striking example (representing cold advection below and warm advection aloft). The display is bisected by a backward "S" between the surface and middle levels; above the middle levels the pattern is reversed by veering winds.

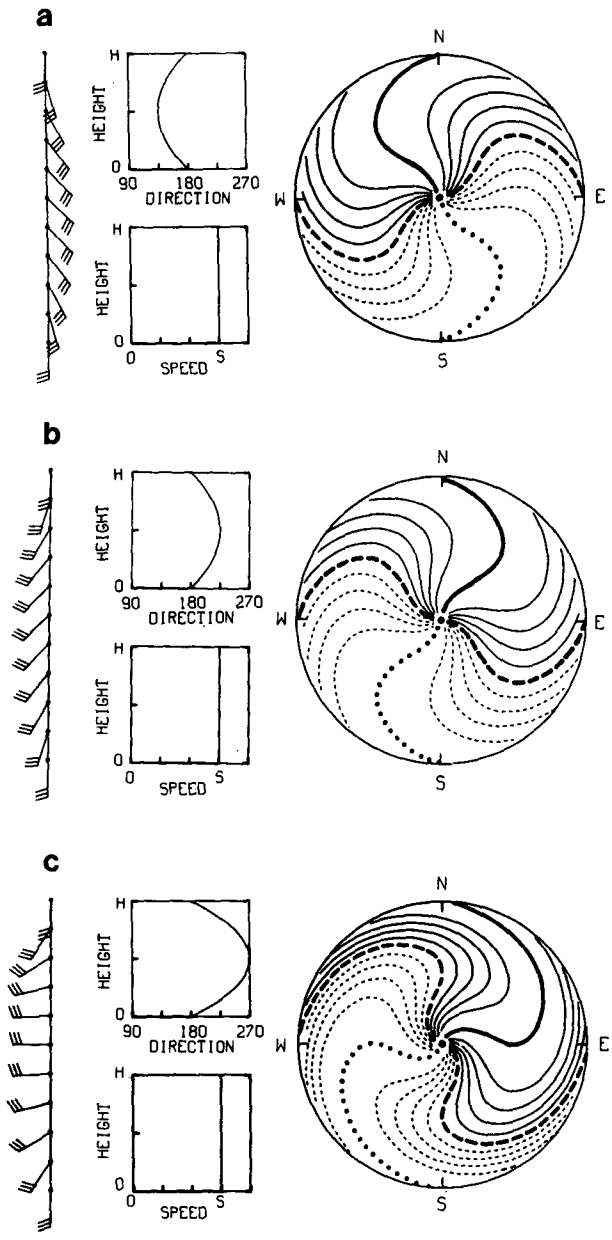

FIG. 6. Nonuniform directional shear with constant wind speed. Doppler velocity contours as in Fig. 3.

Warm advection in the lower layer topped by cold advection aloft is observed in Fig. 6b. This figure resembles Fig. 6a, except that the pattern is reversed; veering winds in the lower level are accompanied by backing winds aloft. The magnitudes of directional

shear of veering and backing winds are indicated by change in the orientation of the zero velocity contour with height (range). Figure 6c has greater curvature than does Fig. 6b. This is due to increased veering of winds up to middle levels accompanied by increased backing of winds aloft.

7. Nonuniform wind speed shear with constant wind direction

In Section 6 we saw the influence of nonuniformity in the environmental wind direction. The following is a discussion of wind speed that varies parabolically with height, as in a jet stream. Figure 7 presents three vertical profiles describing the degree to which the speed changes parabolically with height (range), as given by

$$\left.\begin{aligned} &\text{(a)}\ \mathrm{spd}(h) = S\left[4\frac{h}{H}\left(1-\frac{h}{H}\right)\right] \\ &\qquad \mathrm{dir}(h) = 270^\circ \\ &\text{(b)}\ \mathrm{spd}(h) = S\left[0.5 + 2\frac{h}{H}\left(1-\frac{h}{H}\right)\right] \\ &\qquad \mathrm{dir}(h) = 270^\circ \\ &\text{(c)}\ \mathrm{spd}(h) = S \\ &\qquad \mathrm{dir}(h) = 270^\circ \end{aligned}\right\},\quad 0 \leqslant h \leqslant H. \tag{12}$$

A maximum in the vertical profile of horizontal wind produces a pair of concentric oval-like contours, one upwind and one downwind (Fig. 7a). This feature is due to variation of the wind speed from zero at the ground to a maximum at middle levels and to zero again at the top level. Illustrated in Fig. 7b are contours that tend to converge at the center of the radar display when the surface wind speed is greater than zero. The degree to which the wind speed varies with height (range) can be determined qualitatively by noting the radial gradients in the distribution of Doppler velocity component when the radar is pointing in the direction of the maximum and minimum values. Figure 7a, for instance, indicates stronger west–east wind shear than does Fig. 7b. The weaker the wind shear is, the more rapidly the contours converge until they become straight lines (Fig. 7c), as both wind direction and speed become uniform with height.

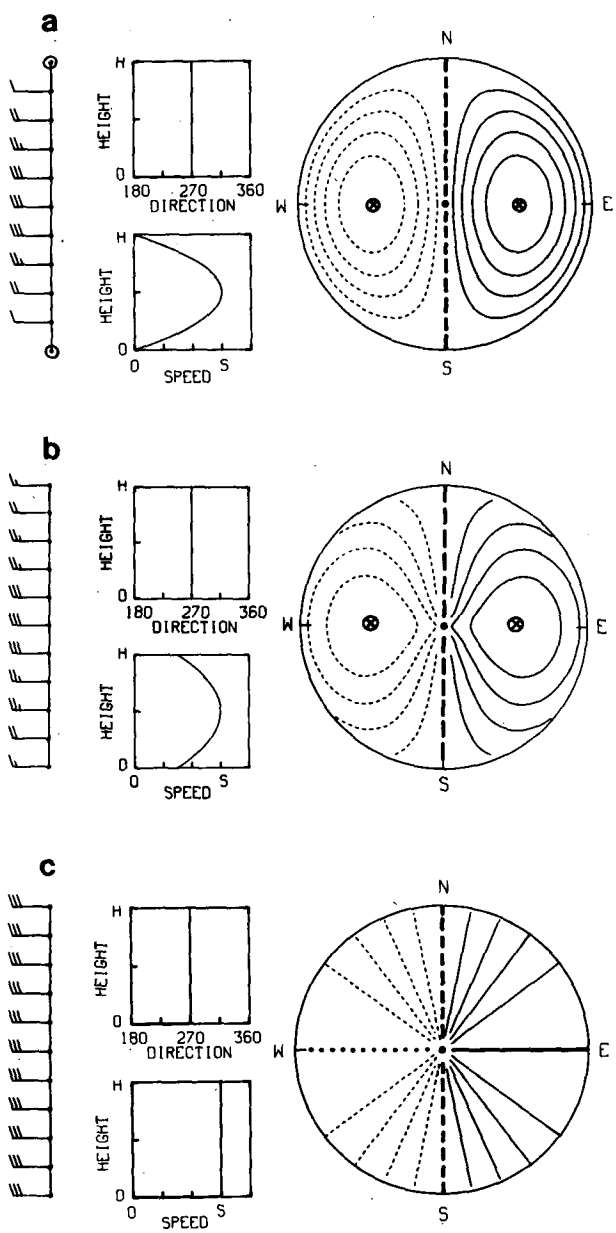

FIG. 7. Nonuniform wind speed shear with constant wind direction. Doppler velocity contours and ×'s as in Fig. 5.

8. Upper- and lower-altitude wind maxima separated by air mass discontinuity

Upper- and lower-altitude wind maxima separated by quasi-horizontal frontal zones commonly are observed in the atmosphere. To investigate single Doppler velocity patterns for wind direction discontinuities of varying degree, we use the following analytical expression for the wind direction profile:

$$\mathrm{dir}(h) = \theta_{h_0} + \theta_w \tanh\left[\frac{\alpha}{H}(h - h_0)\right], \quad \begin{cases} 0 \leqslant h \leqslant H \\ 0 \leqslant h_0 \leqslant H \end{cases} \tag{13}$$

where θ_{h_0} is the wind direction at the midpoint of the frontal zone transition layer (height, h_0), θ_w is half of the wind direction change across the frontal zone, and α is the factor used to strengthen or weaken the gradient across the transition layer. Increasing α leads to a sharper discontinuity in the frontal zone. The frontal surface is assumed to be horizontal over the entire region.

We have observed that a maximum in the vertical profile of horizontal wind speed produces a pair of concentric contours—one upwind and one downwind. Now, we consider two wind speed maxima, one below the height of the frontal zone and the other above. The wind speed profile remains fixed, while the change in wind direction across the zone varies, as described by the expressions

$$\left.\begin{aligned}
&\text{(a)}\quad \mathrm{spd}(h) = S\left[9.71\left(\frac{h}{H}\right) - 17.74\left(\frac{h}{H}\right)^2 - 76.62\left(\frac{h}{H}\right)^3 + 266.75\left(\frac{h}{H}\right)^4 - 271.59\left(\frac{h}{H}\right)^5 + 89.84\left(\frac{h}{H}\right)^6\right] \\
&\qquad \mathrm{dir}(h) = 180° \\
&\text{(b)}\quad \mathrm{spd}(h) = S\left[9.71\left(\frac{h}{H}\right) - 17.74\left(\frac{h}{H}\right)^2 - 76.62\left(\frac{h}{H}\right)^3 + 266.75\left(\frac{h}{H}\right)^4 - 271.59\left(\frac{h}{H}\right)^5 + 89.84\left(\frac{h}{H}\right)^6\right] \\
&\qquad \mathrm{dir}(h) = 180° + 45° \tanh\left[\frac{20}{H}(h - h_0)\right] \\
&\text{(c)}\quad \mathrm{spd}(h) = S\left[9.71\left(\frac{h}{H}\right) - 17.74\left(\frac{h}{H}\right)^2 - 76.62\left(\frac{h}{H}\right)^3 + 266.75\left(\frac{h}{H}\right)^4 - 271.59\left(\frac{h}{H}\right)^5 + 89.84\left(\frac{h}{H}\right)^6\right] \\
&\qquad \mathrm{dir}(h) = 180° + 90° \tanh\left[\frac{20}{H}(h - h_0)\right]
\end{aligned}\right\}, \quad 0 \leq h \leq H \qquad (14)$$

where $h_0 = \dfrac{H}{2}$ is used.

Figure 8a represents an environment with uniform wind direction (straight zero Doppler velocity line) but with a double wind speed maximum. The resulting Doppler velocity pattern contains two upwind maxima and two downwind maxima. When the wind direction changes by 90° across the frontal zone, the pattern in Fig. 8b results. Note the behavior of the zero Doppler velocity contour. Recall that the zero velocity contour represents flow perpendicular to the radar viewing direction; thus, the contour is straight between the center of the radar display and middle levels (middle ranges) before rapidly veering from azimuth 45° (225°) to azimuth 135° (315°). Beyond the middle ranges, the zero velocity contour again becomes straight. Within middle levels the wind direction veers rapidly by 90°, while wind speed decreases to one-third of the maximum value S, indicating the presence of a narrow frontal zone there.

The differences between the Doppler velocity component distributions shown in Figs. 8b and c are apparent. Increasing values of θ_w in Eq. (13) lead to an increased veering of wind direction within the narrow frontal zone. In Fig. 8c where there is a 180° wind shift across the frontal zone, low-level flow is from the east to west, while above the frontal zone, upper-level winds are from the west. In this case, the Doppler velocity contours are packed together in the transition zone as the wind speed changes from S to one-third that value and then back to S again.

9. Surface winds associated with frontal passage

The passage of a surface cold front past a Doppler radar site can be simulated using uniform horizontal wind fields that produce Doppler velocity patterns that resemble those in Fig. 3; Locatelli and Hobbs (1978) describe a similar meteorological situation. The geometry used to simulate the cold front position at zero elevation angle is illustrated in Fig. 9. Equation (13) is modified to represent air mass discontinuity across a vertical frontal zone. The modified equation is

$$\mathrm{dir}(x') = \theta_{x'_0} + \theta_w \tanh\left[\alpha \frac{(x' - x'_0)}{R}\right], \qquad (15)$$

where

$$x' = x\cos\psi + y\sin\psi,$$

and $\theta_{x'_0}$ is the wind direction at the midpoint of the frontal zone x'_0, θ_w is half of the wind direction change across the zone, α is the factor used to strengthen the frontal gradient, R is the maximum range at the edge of the radar display, and ψ is the angle through which the x', y' coordinate system is rotated in order for the y' axis to become parallel to the front.

The right column of Fig. 10 illustrates an idealized representation of the single Doppler velocity pattern in the vicinity of a passing cold front. The corresponding vector field shown on the radar display format is exhibited in the left column. In order to simulate the cold front approaching from the northwest and passing through the radar site, the locations of the front are $x'_0 = -X'/2$, 0, $+X'/2$. The front is indicated by light stippling as shown in Fig. 10. Behind the front, the surface wind is assumed to be westerly; ahead of the front, the wind is southwesterly. Parameters used to specify the frontal features are $\theta_{x'_0} = 247.5°$, $\theta_w = -22.5°$, $\alpha = 50$ and $\psi = 315°$.

The most significant Doppler velocity feature in Fig. 10 is the packing of the contours in the frontal zone

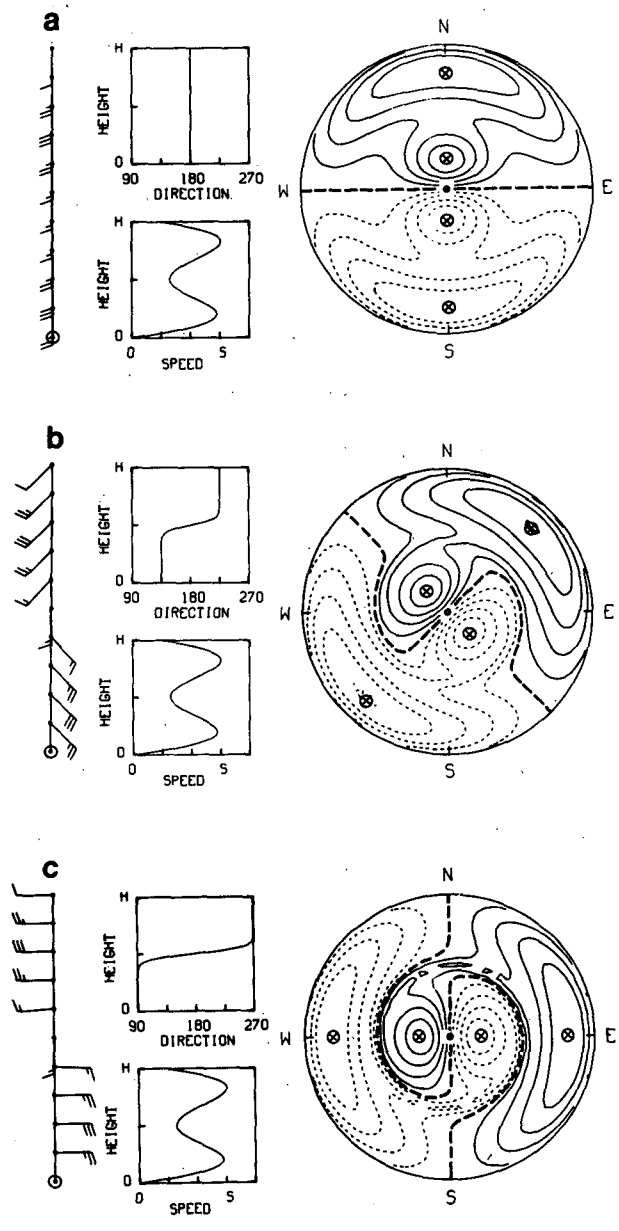

FIG. 8. Upper- and lower-altitude wind maxima separated by air mass discontinuity. Doppler velocity contours and X's as in Fig. 5.

when the front is not located over the radar site. The frontal zone also is characterized by a marked discontinuity in the isopleths. The zero Doppler velocity contour is a very useful indicator of wind direction; one notes wind approaching the radar from the southwest ahead of the front and approaching it from the west behind the front.

One can visualize how Doppler velocity fields would look at higher elevation angles by assuming that one wind profile in Figs. 4–7 represents the wind on one side of the front and another profile represents the wind on the other side. For example, uniformly strong southerly winds that veer with height ahead of the front and a low-level westerly jet behind the front would consist of the curved contours of Fig. 4b ahead of the front and the nearly concentric contours of Fig. 7b behind it.

10. Comparison with actual Doppler velocity displays

Baynton et al. (1977) and Wilson et al. (1980) described how their color displays may be used to interpret data obtained from widespread precipitation systems. Kraus and Donaldson (1976) prepared a simulated display of the Doppler velocity field based on hypothetical vertical profiles of wind speed and direction. Their interpretations of the field are like ours. In this section, we use uniform flow models to simulate actual single Doppler velocity observations in situations of optically clear air and widespread precipitation.

a. Stratiform precipitation

Wilson et al. (1980) used color displays of single Doppler radial velocity patterns to interpret California wintertime stratiform precipitation in real time. In Fig. 11a, adapted from Wilson et al., closed contours representing upper- and low-levels of jet-like flow are evident. The upper-level velocity maximum slopes upward toward the east-northeast, appearing at a greater slant range downwind than upwind. This is due to upward sloping terrain toward the Sierras to the east. The south-southeast direction of the low-level jet is, at least in part, the result of channeled winds parallel to the Sierra Nevada under stably stratified conditions, according to Wilson et al. (1980).

The most distinguishable feature in Fig. 11a is an S-shaped zero Doppler velocity band (representing velocities from +3 to −3 m s^{-1}). The winds veer with height from the lowest level to near the middle range

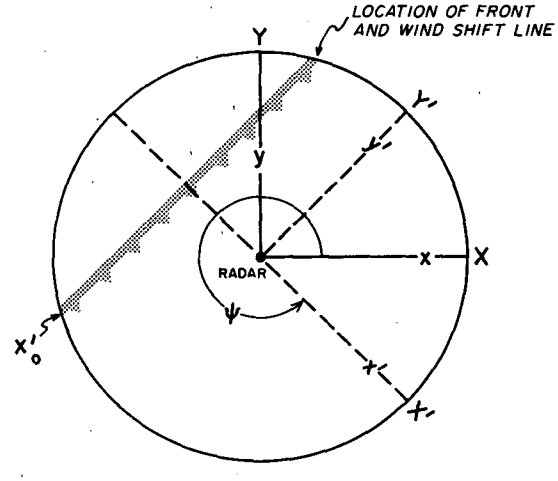

FIG. 9. The geometry of a surface cold front position (light stippling) relative to a Doppler radar site. The x', y' axes which are relative to the front are rotated through an angle ψ from the x, y coordinate system. (After Locatelli and Hobbs, 1978.)

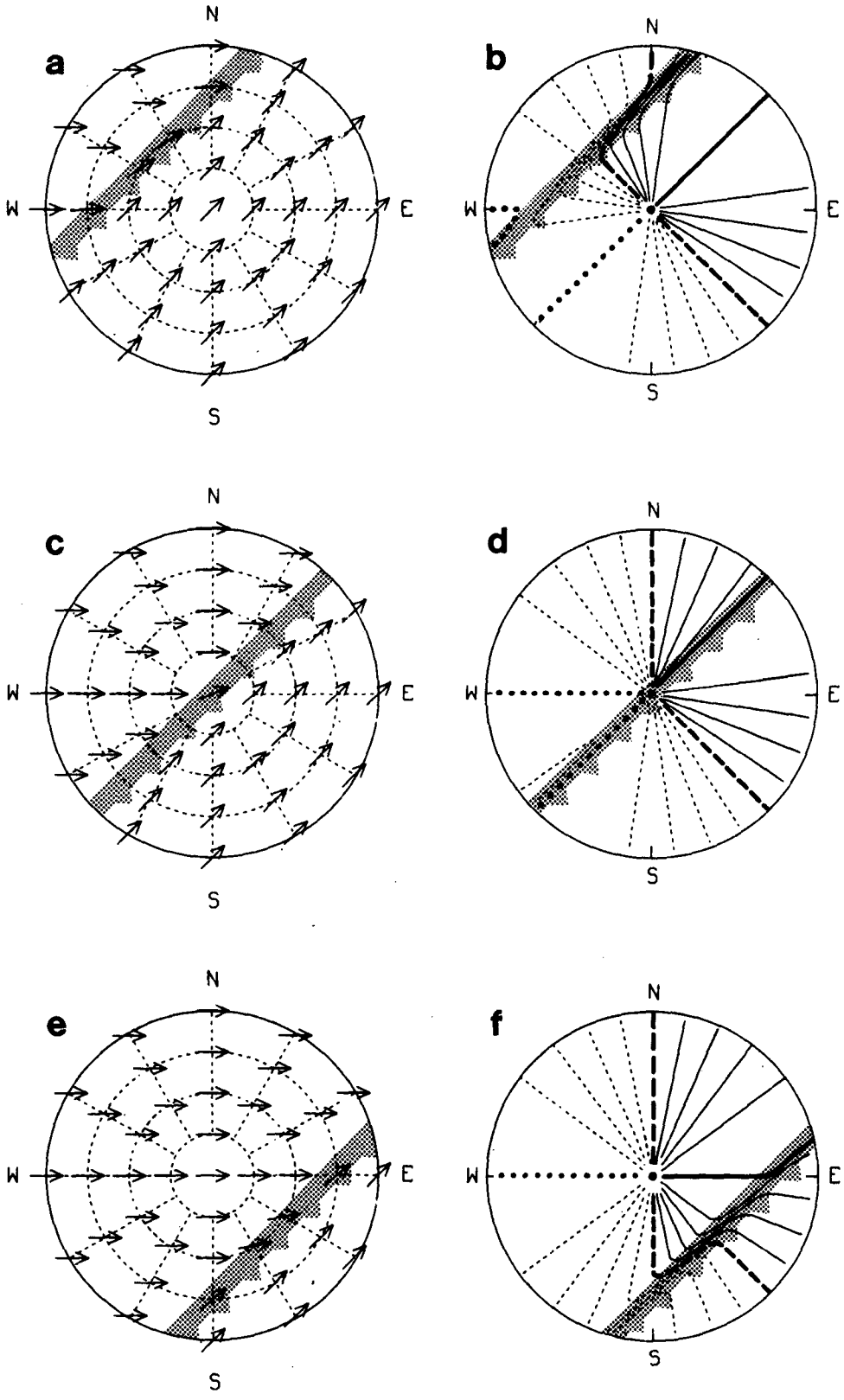

FIG. 10. The left column (a, c, e) represents wind vector fields in the vicinity of a surface cold front (shown on radar display format) The right column (b, d, f) represents the corresponding single Doppler velocity patterns at zero elevation angle. Doppler velocity contours as in Fig. 3. The front is indicated by light stippling.

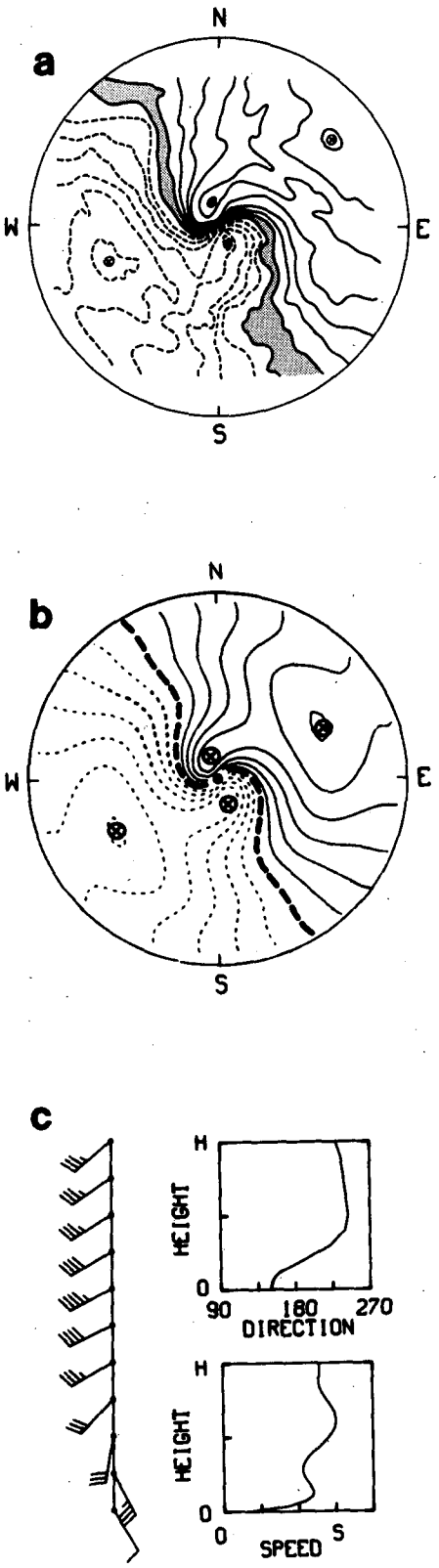

FIG. 11. (a) Doppler velocity pattern measured at 0930 PST on 7 February 1978 near Sacramento, California. Elevation angle is 9.5°. Stippled area is zero Doppler velocity band ranging from −3 to +3 m s^{-1}. Contour interval is 6 m s^{-1}. Solid contours are velocities away from radar; dashed contours are velocities toward radar. Velocity extremes are measured at circled ×'s. (After Fig. 3b of Wilson et al., 1980.) (b) Simulated Doppler velocity pattern based on (c). Heavy dashed line is zero velocity contour. Contour interval is 0.2 S. Contours same as in Fig. 11a. (c) Modeled wind speed and direction profiles based on Doppler-derived winds. Maximum wind speed S is 41 m s^{-1}; maximum height H is 6.7 km. Full wind barb represents 10 m s^{-1}.

of the radar display, indicative of strong warm advection throughout this layer. Near the edge of the display, winds backing with height indicate that cold air is being advected into the region.

Figure 11b shows the simulation of Fig. 11a using a mean vertical profile of uniform horizontal winds (Fig. 11c). A least-squares data fit to the wind profile deduced from Fig. 11a results in the following expressions for wind speed and direction

$$\left.\begin{aligned}\mathrm{spd}(h) &= S\left[0.25 + 12.37\left(\frac{h}{H}\right) - 96.96\left(\frac{h}{H}\right)^2 + 328.43\left(\frac{h}{H}\right)^3 - 529.52\left(\frac{h}{H}\right)^4 + 403.97\left(\frac{h}{H}\right)^5 - 117.71\left(\frac{h}{H}\right)^6\right] \\ \mathrm{dir}(h) &= 149.6^\circ\left[1 - 2.4\left(\frac{h}{H}\right) + 36.4\left(\frac{h}{H}\right)^2 - 118.1\left(\frac{h}{H}\right)^3 + 170.6\left(\frac{h}{H}\right)^4 - 116.8\left(\frac{h}{H}\right)^5 + 30.9\left(\frac{h}{H}\right)^6\right]\end{aligned}\right\}, \quad 0 \leq h \leq H \quad (16)$$

where S is the maximum wind speed of 41 m s^{-1} and H = 6.7 km. In Eq. (16), the directional value of 149.6° is the surface wind direction at the height of the radar.

There is a similarity between the measured and simulated patterns in Figs. 11a and 11b. Some of the differences are attributed to the simplifying assumptions and to the lack of taking precipitation vertical velocities into account.

b. Frontal discontinuity in a stratiform snowstorm

On 31 January 1984, the Air Force Geophysics Laboratory's 10 cm-wavelength Doppler radar in Sudbury, Massachusetts monitored a New England stratiform snowstorm. A low pressure system was rapidly advancing toward the northeast along the New England coastline. Figure 12a illustrates the Doppler velocity display extracted from the real-time color display for 0231 EST (Mike Istok, NEXRAD staff, personal communication, 1984). At that time, the low pressure sys-

tem was located to the south-southeast of the radar site.

The zero Doppler velocity band shown in Fig. 12a represents velocities from +1 to −1 m s^{-1}. Near the radar site, the band is oriented northeast–southwest, indicating low-level wind flow from the southeast. Also evident is a pair of concentric contours, one upwind and one downwind, indicative of low-level wind maxima. Above the height of the low-level maxima, the zero Doppler velocity band rapidly veers and then backs with height until it traces a quasi-straight line extending to the edge of the echo. It is believed that a frontal discontinuity exists in the layer where the wind direction abruptly changes from east-southeast to west-southwest.

A single sixth-order polynomial does not fit the observed profile of wind direction, because of the rapid changes through and immediately above the frontal zone. An alternative method is to divide the entire layer into three sublayers corresponding to the extreme variations of the wind direction with height. Fitting the profiles with sixth-order polynomials (Fig. 12c) gives the following expressions for wind speed and direction up to 6.7 km:

$$\left.\begin{aligned}
\mathrm{spd}(h) &= S\left[4.12\left(\frac{h}{H}\right) - 32.25\left(\frac{h}{H}\right)^2 + 95.82\left(\frac{h}{H}\right)^3 - 125.72\left(\frac{h}{H}\right)^4 + 76.93\left(\frac{h}{H}\right)^5 - 17.92\left(\frac{h}{H}\right)^6\right], \\
&\qquad\qquad 0 \leqslant h \leqslant H \\
\mathrm{dir}(h) &= 106.4^\circ\left[1 + 0.57\left(\frac{h}{H}\right) + 8.3\left(\frac{h}{H}\right)^2 + 2.97\left(\frac{h}{H}\right)^3 - 614.4\left(\frac{h}{H}\right)^4 + 118.82\left(\frac{h}{H}\right)^5 + 16688.84\left(\frac{h}{H}\right)^6\right], \\
&\qquad\qquad 0 \leqslant h \leqslant 0.2H \\
\mathrm{dir}(h) &= 170^\circ\left[-178.57 + 2764.71\left(\frac{h}{H}\right) - 14807.76\left(\frac{h}{H}\right)^2 + 23035.62\left(\frac{h}{H}\right)^3 + 66111.28\left(\frac{h}{H}\right)^4\right. \\
&\qquad \left. - 276497.82\left(\frac{h}{H}\right)^5 + 271141.88\left(\frac{h}{H}\right)^6\right], \quad 0.2H \leqslant h \leqslant 0.325H \\
\mathrm{dir}(h) &= 203.1^\circ\left[11.83 - 98.17\left(\frac{h}{H}\right) + 352.52\left(\frac{h}{H}\right)^2 - 649.05\left(\frac{h}{H}\right)^3 + 651.43\left(\frac{h}{H}\right)^4\right. \\
&\qquad \left. - 339.45\left(\frac{h}{H}\right)^5 + 71.98\left(\frac{h}{H}\right)^6\right], \quad 0.325H \leqslant h \leqslant H
\end{aligned}\right\} \tag{17}$$

where the maximum wind speed S is 49 m s^{-1}. The result is the strikingly similar synthetic Doppler wind field shown in Fig. 12b.

11. Conclusions

A variety of wind information in a nondivergent environment, usually easily identified by single Doppler velocity patterns, is presented. Such information can be useful in providing a nowcaster and/or forecaster with a real-time physical understanding of weather events. This is especially important with the coming of NEXRAD. Representative samples of single Doppler velocity patterns that can be found in optically clear air and in widespread precipitation are summarized in Fig. 13. The signatures are divided into four wind speed and three direction categories that represent the main environmental conditions discussed. These categories should help to make "order out of the chaos" that one may have experienced while trying to assimilate the wind information in Figs. 3–8.

When wind speed is constant (nonzero) with height (left column of Fig. 13) all Doppler velocity contours pass through the radar location at the center of the display. Also, maximum and minimum Doppler velocities occur all along the heavier (nonzero) contour lines rather than just at one point (circled ×'s) as with other wind speed profiles.

When wind speed is not zero at the ground, contour lines representing wind speed magnitudes less than or equal to the surface value pass through the radar location at display center (as seen in Figs. 13a, e and i). When the surface speed is zero (other three columns in Fig. 13), only the zero Doppler velocity contour (thick, long dashes) passes through the center of the radar display.

If the wind speed profile has a peak within the height interval on the display, there will be a pair of closed contours 180° from each other; the azimuth of the minimum is the direction from which the velocity jet is approaching the radar, and the height of the peak value can be computed from the radar antenna's ele-

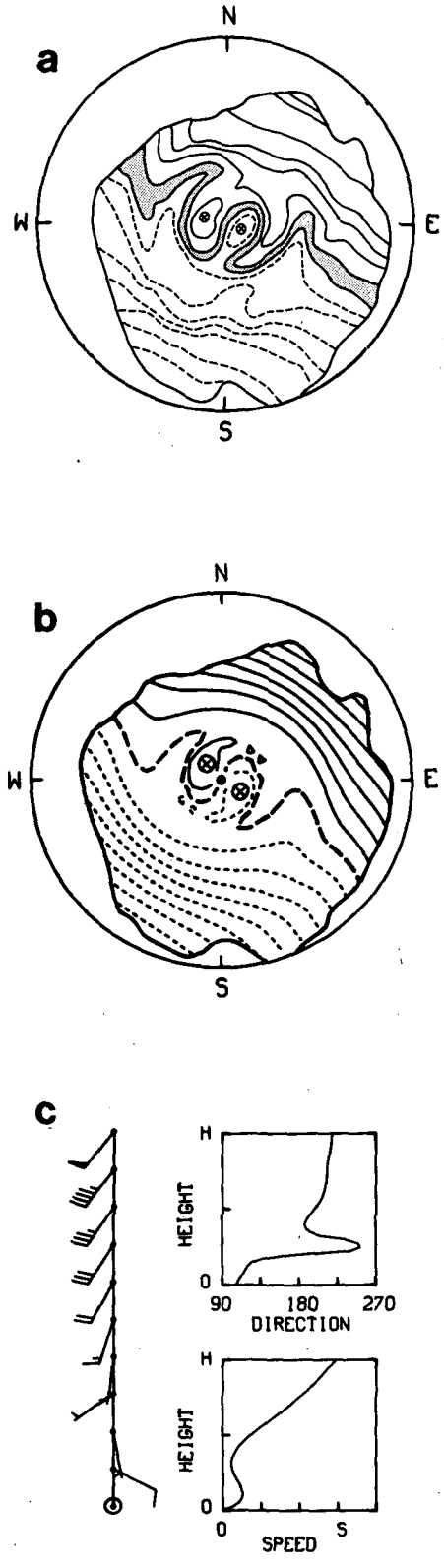

FIG. 12. (a) Doppler velocity pattern measured at 0231 EST on 31 January 1984 at the Air Force Geophysics Laboratory's radar in Sudbury, Massachusetts. Elevation angle is 3.8°. Stippled area is zero Doppler velocity band ranging from −1 to +1 m s^{-1}. Contour interval is 4.67 m s^{-1}. Contours same as in Fig. 11. (Provided by Mike Istok, NEXRAD staff, personal communication, 1984.) (b) Simulated Doppler velocity pattern based on (c). Contour interval is 0.1 S. Contours same as in Fig. 11. (c) Modeled wind speed and direction profiles based on Doppler-derived winds. Maximum wind speed S is 49 m s^{-1}; maximum height H is 6.7 km. Full wind barb represents 10 m s^{-1}.

vation angle and the slant range (r_s) to that point. This feature is evident in Figs. 13c, g and k.

Whereas the wind speed profile controls the overall pattern including the spacing between contours, the vertical profile of wind direction controls contour curvature. The most informative contour for wind direction is the zero velocity contour (thick, long dashes). Note that the zero contours are identical in each row (reflection of wind direction profile) even though the overall patterns in each row differ significantly (reflection of wind speed profile).

Since wind direction is perpendicular to a radial line (from display center) at the point where the line intersects the zero velocity contour, wind direction variation with height (range on the radar scope) can be determined by inspection. Air motion is from the negative (thin dashed lines) side of the zero contour toward the positive (thin solid lines) side. Looking at the middle row (Figs. 13e, f, g and h), we see that there are southerly winds at the ground—the zero velocity line is oriented east–west and air is approaching from the south and flowing away toward the north. Halfway between the center and edge of the display, southwesterly winds are perpendicular to a radial line. At the edge of the display, wind is from the west because the radial line intersecting the zero contour is oriented north–south.

Veering winds, representative of warm air advection, produce a striking S-shaped pattern on the Doppler zero velocity contours, whereas backing winds, representative of cold air advection, produce a backward S. These features are seen in the middle and bottom rows.

Sharp wind shifts frequently are associated with frontal boundaries. The sharp bend in the zero velocity contour and close packing of the contours indicate the presence of a frontal surface. Thus, low-altitude measurements can be used to precisely locate and track the movement of frontal boundaries.

We have shown that various wind speed and direction profiles produce unique single Doppler velocity patterns (signatures) in a PPI scope display. These signatures can be used by operational meteorologists to identify the current wind conditions through a considerable depth of the atmosphere. More importantly, one is able to recognize when the wind field is evolving and when frontal discontinuities are passing the radar coverage area. Thus, the ability to interpret Doppler velocity displays will be important to the operational community of the future.

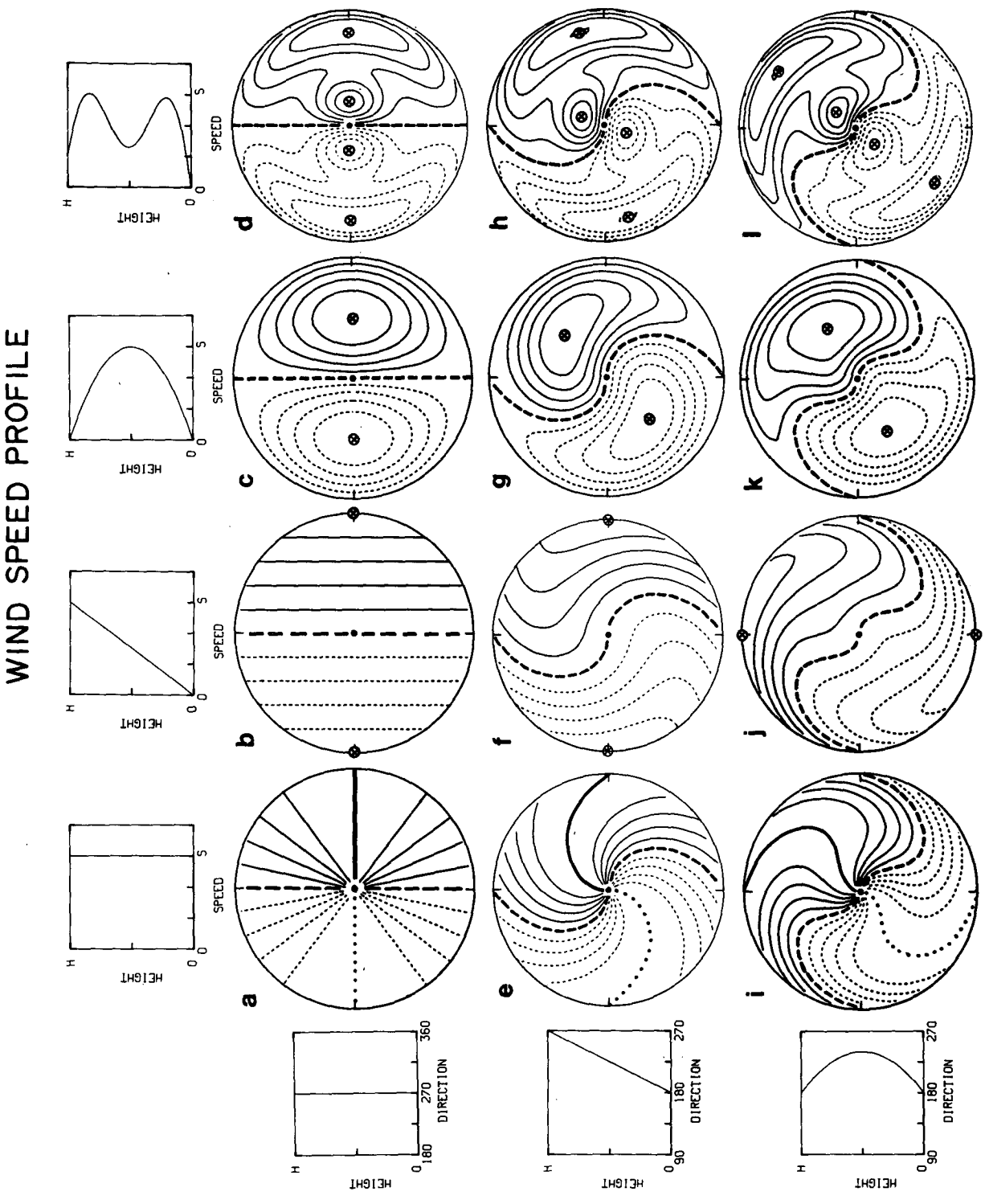

FIG. 13. Doppler velocity patterns (PPI scans at constant elevation angle) for various vertical profiles of wind speed and direction. Contour interval is 0.2 S. Contours as in Figs. 3 and 5.

Acknowledgments. We appreciate the assistance of Michael Anderson and Louis Wicker in running the computer programs that produced the simulated flow fields. Mike Istok provided the real-time Doppler color display described in Section 12b. Joan Kimpel expertly drafted those figures that were not produced by computer. Photographic reduction of figures was efficiently performed by Robert Goldsmith. Sandra McPherson and Michelle Foster are to be commended for their perseverance in handling the various drafts of the manuscript. This work was partially supported by NEXRAD Contract NA-82-SAC-00761 to the University of Oklahoma.

REFERENCES

Baynton, H. W., 1979: The case for Doppler radars along our hurricane-affected coasts. *Bull. Amer. Meteor. Soc.*, **60,** 1014–1023.

——, R. J. Serafin, C. L. Frush, G. R. Gray, P. V. Hobbs, R. A. Houze, Jr. and J. D. Locatelli, 1977: Real-time wind measurement in extratropical cyclones by means of Doppler radar. *J. Appl. Meteor.*, **16,** 1022–1028.

Bonewitz, J. D., 1981: The NEXRAD program—An overview. Preprints, *20th Conf. Radar Meteorology,* Boston, Amer. Meteor. Soc., 757–761.

Browning, K. A., and R. Wexler, 1968: A determination of kinematic properties of a wind field using Doppler radar. *J. Appl. Meteor.*, **7,** 105–113.

Gray, G. R., R. J. Serafin, D. Atlas, R. E. Rinehart and J. Boyajian, 1975: Real-time color Doppler radar display. *Bull. Amer. Meteor. Soc.*, **56,** 580–588.

JDOP Staff, 1979: *Final Report on the Joint Doppler Operational Project (JDOP), 1976–1978.* NOAA Tech. Memo. ERL NSSL-86, Natl. Severe Storms Lab., Norman, 84 pp. [NTIS, PB80-107188/AS]

Johannessen, K., and E. Kessler, 1976: Program to develop Doppler radar for use in the National Weather Service. Preprints, *17th Conf. Radar Meteorology,* Boston, Amer. Meteor. Soc., 560–561.

Kraus, M. J., and R. J. Donaldson, Jr., 1976: Interpolation of PPI velocity displays in widespread storms. Preprints, *17th Conf. Radar Meteorology,* Boston, Amer. Meteor. Soc., 239–243.

Lhermitte, R. H., and D. Atlas, 1961: Precipitation motion by pulse-Doppler radar. Preprints, *9th Conference on Radar Meteorology,* Boston, Amer. Meteor. Soc., 218–223.

Locatelli, J. D., and P. V. Hobbs, 1978: A technique for obtaining detailed wind fields in a frontal system from a single-Doppler radar. *J. Appl. Meteor.* **17,** 1076–1079.

Rabin, R., and D. Zrnić, 1980: Subsynoptic-scale vertical wind revealed by dual Doppler-radar VAD analysis. *J. Atmos. Sci.*, **37,** 644–654.

Ray, P. S., and K. Colbert, (Eds.), 1982: *Proc. of the NEXRAD Doppler Radar Symposium/Workshop.* Cooperative Institute for Mesoscale Meteorological Studies, University of Oklahoma, Norman, 235 pp.

Wilson, J. W., 1982: Single Doppler observations for forecasting and warning. *Proc. of the NEXRAD Doppler Radar Symposium/Workshop.* P. S. Ray and K. Colbert, Eds., Cooperative Institute for Mesoscale Meteorological Studies, University of Oklahoma, Norman, 6–30.

——, R. E. Carbone, H. W. Baynton and R. J. Serafin, 1980: Operational application of meteorological Doppler radar. *Bull. Amer. Meteor. Soc.*, **61,** 1154–1168.

Wood, V. T., and R. A. Brown, 1983: Single Doppler velocity signatures: An atlas of patterns in clear air/widespread precipitation and convective storms. NOAA Tech. Memo. ERL NSSL-95, Natl. Severe Storms Lab., Norman, 71 pp. [NTIS PB84155779]